Memory capacity of adaptive flow networks

Komal Bhattacharyya,[1] David Zwicker,[1] and Karen Alim[1,2,*]
[1]*Max Planck Institute for Dynamics and Self-Organisation, 37077 Göttingen, Germany*
[2]*Center for Protein Assemblies and Department of Bioscience, School of Natural Sciences, Technische Universität München, 85748 Garching, Germany*

(Received 4 August 2022; accepted 9 February 2023; published 30 March 2023)

Biological flow networks adapt their network morphology to optimize flow while being exposed to external stimuli from different spatial locations in their environment. These adaptive flow networks retain a memory of the stimulus location in the network morphology. Yet, what limits this memory and how many stimuli can be stored are unknown. Here, we study a numerical model of adaptive flow networks by applying multiple stimuli subsequently. We find strong memory signals for stimuli imprinted for a long time into young networks. Consequently, networks can store many stimuli for intermediate stimulus duration, which balance imprinting and aging.

DOI: 10.1103/PhysRevE.107.034407

I. INTRODUCTION

Biological flow networks, such as vasculature [1], fungal mycelium [2], or slime mold [3,4], optimize their function by remodeling the network morphology in response to internal and external stimuli [3,5–10]. In particular, the slime mold *Physarum polycephalum* reorganizes its network morphology during foraging and migration [11,12], or as responses to environmental influences [13], by adapting tubes to flow [8,9,14]. Although the organism only consists of a single cell, it processes information [8,9,15–18] and stores memory of external stimuli in the network morphology [13,19]. Yet, the information processing capabilities of *Physarum* in particular, and adaptive flow networks more generally, are so far unclear.

The self-organized information processing of *Physarum* is reminiscent of other physical learning systems [20]: Physical networks can be trained to have unusual mechanical properties [21,22] and functionalities [23,24], either by modifying microscopic properties by global optimization [25] or as local responses [26]. Such networks can also learn multiple states [27], which is key for obtaining multifunctionality [27] and multistability [28–37] in physical systems, and for performing complex tasks such as image classification [38–40] using such physical networks. The multiple states can be either imprinted simultaneously [27] or learned subsequently [38]. In both cases, there is a maximal number of states that can be learned, which is the learning capacity of the system [27,38].

Although memory is essential for learning [20], the memory capacity of flow networks remains relatively unexplored. Here, we investigate this question theoretically by analyzing memory in a model of adaptive flow network, which is subjected to various external stimuli, similar to natural flow networks [41,42]. We identify that a stimulus is stored more robustly, and can thus be retrieved more easily, when networks are young and are exposed to a stimulus for a long time. Since these two criteria are incommensurable for multiple stimuli, a trade-off determines the memory capacity of these adaptive flow networks.

II. MODEL

We use the standard model for adaptive flow networks that minimizes energy dissipation, for a fixed network building material [1,43–47]. These flow networks are modeled as a graph of N_{nodes} nodes connected by links ij, where $i, j \in \{1, \ldots, N_{\text{nodes}}\}$. The links have length l_{ij} and time-dependent conductances $C_{ij}(t)$. We consider a network of cylindrical hollow tubes with conductances $C_{ij} = \pi r_{ij}(t)^4/8\mu l_{ij}$ according to Hagen-Poiseuille's law, where r_{ij} is the radius of the tube and μ is the viscosity of the enclosed fluid. In our case, node $i = 1$ serves as the sole outlet, while all other nodes are inlets, following models of flow networks in plants and animals [45–47]. The inlets are modeled with fluctuating inflows $q_i(t)$, which are either $q_i = 0$ or $q_i = 2q^{(0)}$ with equal probability. These switchlike fluctuations represent inflow fluctuations observed in both plants [45,48] and animals [7,49–51]. Conservation of total flow implies $q_1(t) = -\sum_{i>1} q_i(t)$. We chose a disk-shaped network geometry with the outlet in the center to maximize symmetry; see Fig. 1(a). Conservation of flow at every node, described by Kirchhoff's law, then uniquely determines the flow $Q_{ij}(t)$ in all links, given the entire network's conductances $C_{ij}(t)$ and the inflows $q_i(t)$; see the Supplemental Material [52], Sec. I. The adaptive dynamics follow from the assumption that networks minimize

*k.alim@tum.de

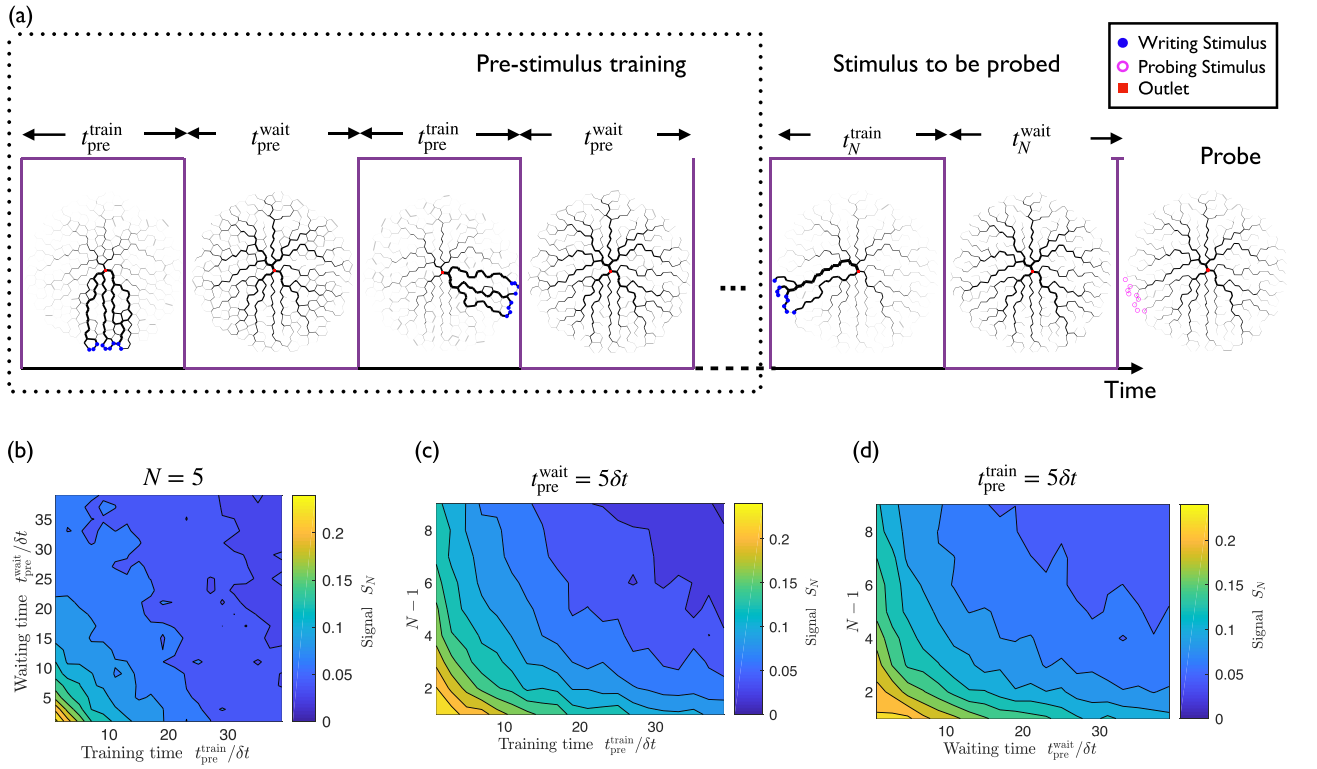

FIG. 1. Stimulus locations are retained in previously stimulated networks. (a) Schematic of adaptive flow networks with a central outlet (red square), fluctuating inflows at all other nodes, and additional inflow for stimuli (blue filled circles). The temporal sequence shows snapshots of the training protocol, where N stimuli (purple boxes) are applied sequentially by stimulating for a period t_n^{train} followed by relaxation period t_n^{wait} for each stimulus. Finally, the last stimulus is probed (pink unfilled circles) to determine the signal S_N according to Eq. (4). (b) S_N as a function of the training time $t_n^{\text{train}} = t_{\text{pre}}^{\text{train}}$ and waiting time $t_n^{\text{wait}} = t_{\text{pre}}^{\text{wait}}$ for most stimuli ($n < N$) with $N = 5$. (c) S_N as a function of $t_{\text{pre}}^{\text{train}}$ and N for $t_{\text{pre}}^{\text{wait}} = 5\delta t$. (d) S_N as a function of $t_{\text{pre}}^{\text{wait}}$ and N for $t_{\text{pre}}^{\text{train}} = 5\delta t$. (a)–(d) Model parameters are $t_N^{\text{train}} = 10\delta t$, $t_N^{\text{wait}} = 5\delta t$, $N_{\text{nodes}} = 1100$, $q^{\text{add}} = 2000\, q^{(0)}$, $q^{(0)} = 1$, $\mathcal{K} = 1600$, and $T = 30\delta t$. Data show mean from 1500 independent simulations.

dissipation [1],

$$E(t) = \sum_{<ij>} \frac{Q_{ij}(t)^2}{C_{ij}(t)}, \tag{1}$$

while obeying the constraint

$$\mathcal{K}^{\frac{1}{2}} = \sum_{\langle ij \rangle} C_{ij}(t)^{\frac{1}{2}} l_{ij}^{\frac{3}{2}}, \tag{2}$$

where $\mathcal{K}^{\frac{1}{2}}$ is proportional to the fixed overall volume of all links. We follow an iterative relaxation algorithm [44,45], where the conductances at the next time step, $C_{ij}(t+\delta t)$, adapt to minimize $E(t)$ while obeying Eq. (2), implying

$$C_{ij}(t+\delta t) = \frac{\mathcal{K} \langle Q_{ij}(t)^2 \rangle_T^{\frac{2}{3}}}{\left(\sum_{\langle ij \rangle} \langle Q_{ij}(t)^2 \rangle_T^{\frac{1}{3}} l_{ij} \right)^2 l_{ij}}, \tag{3}$$

where we average the flow over a duration T, $\langle Q_{ij}^2 \rangle_T$, since the inflows at every node fluctuate over time.

To probe for memory, we initiate networks with conductances C_{ij} chosen uniformly from the interval $[0, 1]$, which are then rescaled, so they obey the constraint given by Eq. (2). We then stimulate the networks using an additional inflow q^{add} at the outer rim at a specific angular location; see Fig. 1(a). Such stimuli are comparable to stimuli used when observing memory in *Physarum* [13]. We distribute the additional inflow over a few nodes to avoid artifacts from the symmetries of the underlying networks. The adaptation dynamics then imprint the stimulus in a treelike structure from the nodes of additional inflow to the centered outlet [19]; see Fig. 1(a). Once the additional inflow is withdrawn, networks return to seemingly isotropic morphologies. Yet, when probing networks by reapplying an additional load at exactly the same location, the power loss of previously stimulated, and thus trained, networks, E_{trained}, is distinctively less than if probed at any other location; see the Supplemental Material [52], Sec. II. In particular, E_{trained} is less than the power loss $E_{\text{untrained}}$ for probing untrained networks that evolved for the same total time, but did not see the stimulus [19]. To quantify this memory, we established the normalized difference in power loss between trained and untrained networks as a measure of the memory readout signal S [19],

$$S = 1 - \frac{\langle E_{\text{trained}} \rangle}{\langle E_{\text{untrained}} \rangle}, \tag{4}$$

where brackets indicate ensemble averages over initial configurations and positions of the additional loads; see the Supplemental Material [52], Sec. II. We used this quantification to show that freshly initiated networks memorize single

stimuli in the spatial location and orientation of the vanishing links [19]. The stimulus can be read out by probing the network again after the stimulus is withdrawn. Yet, it is unclear how well already stimulated networks can store stimuli and whether networks can store multiple stimuli simultaneously.

III. RESULTS

A. Prestimulated networks can memorize stimuli

We start by asking whether previously evolved networks can store a stimulus reliably. We evolve networks with a stimulation protocol by consecutively applying N stimuli, distinguished by the angle of the additional inflow. We choose the angles randomly from 10 possibilities, $\{0, \frac{\pi}{5}, \ldots, \frac{9\pi}{5}\}$, and we set the angular range of each stimulus to $\frac{\pi}{6}$ to avoid stimuli overlap. Starting with a randomly initialized network, we apply one stimulus after the other. The nth stimulus is imprinted on the network by iterating Eq. (3) with the additional load corresponding to the stimulus for a duration t_n^{train} and then without load for a duration t_n^{wait}. Taken together, the network evolves to time

$$t_n^{\text{age}} = \sum_{m=1}^{n} \left(t_m^{\text{train}} + t_m^{\text{wait}}\right), \tag{5}$$

after the nth stimulus has been applied.

To test whether a stimulated network can memorize an additional stimulus, we apply $N-1$ stimuli with identical properties and then probe the signal of a final stimulus; see Fig. 1(a). We thus have $t_n^{\text{train}} = t_{\text{pre}}^{\text{train}}$ and $t_n^{\text{wait}} = t_{\text{pre}}^{\text{wait}}$ for $n < N$, while the final stimulus can have different parameters. The signal S_N quantifies the dissipation difference of applying the Nth stimulus, analogously to Eq. (4). For constant parameters of the prestimulation protocol, we observe that S_N increases with t_N^{train} and decays with t_N^{wait}; see the Supplemental Material [52], Sec. III. This behavior closely resembles memory formation in a freshly initiated network [19], even though here we use prestimulated networks.

We next test the influence of the precise prestimulation protocol by varying the number of applied stimuli, N, the training time $t_{\text{pre}}^{\text{train}}$, and the relaxation time $t_{\text{pre}}^{\text{wait}}$. Figures 1(b)–1(d) show that the signal S_N of the final stimulus decreases when increasing any of these parameters, so the prestimulation protocol affects how well additional memories can be stored. However, our simulations demonstrated that prestimulated adaptive networks can store information about additional stimuli.

B. Memory capacity reduces with age

We next investigate how the prestimulation protocol affects the memory of the final stimulus. Since information about stimuli locations is stored in the orientation and location of irreversibly decaying links [19], we first determine how the microstructure of the network evolves with time. Figure 2(a) shows that the average fraction of vanishing links saturates exponentially with time (independent of the choice of fluctuations of inflows; see the Supplemental Material [52], Sec. IV), which suggests that the memory capacity of adaptive flow networks decreases with the time t_{N-1}^{age}, given by Eq. (5), that the network evolved for before the stimulus is applied. Replotting the memory signal S_N of the final stimulus as a function of t_{N-1}^{age} leads to a data collapse for various values of N, $t_{\text{pre}}^{\text{train}}$, and $t_{\text{pre}}^{\text{wait}}$; see Figs. 2(b) and 2(c). The two panels differ in whether N [Fig. 2(b)] or $t_{\text{pre}}^{\text{wait}}$ [Fig. 2(c)] are kept fixed while the other parameters are varied. In both cases, the data collapse is well

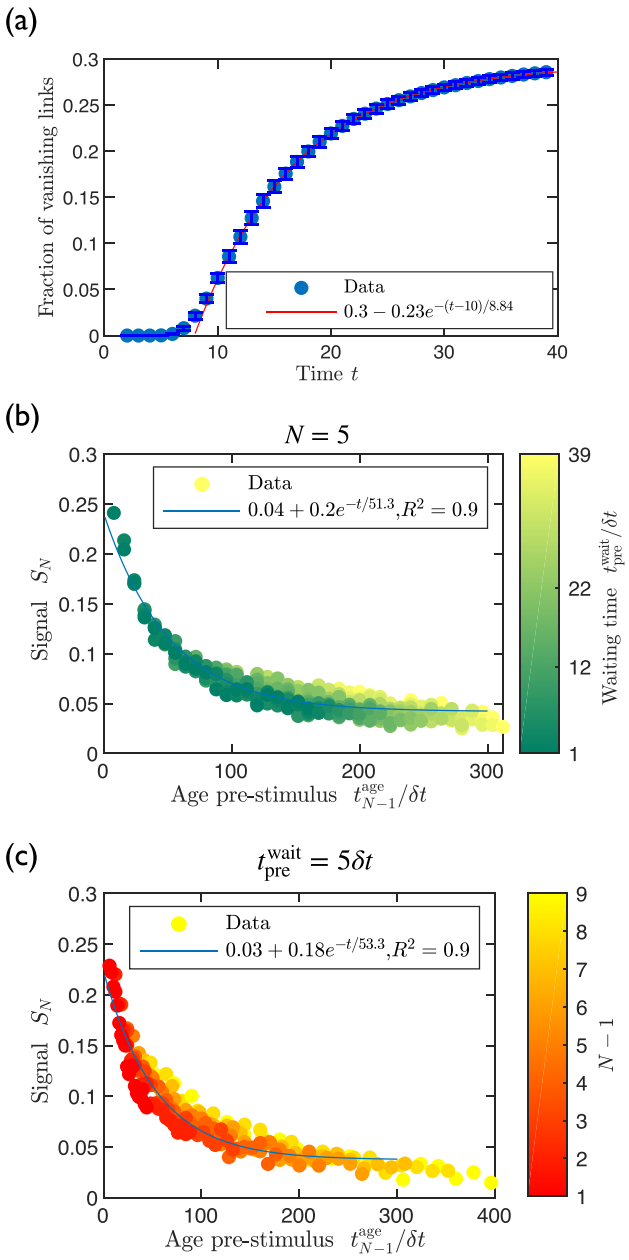

FIG. 2. Memory signal of final stimulus reduces with network age. (a) Fraction of vanishing links (blue symbols) as a function of network iterations averaged over 80 independent runs. Model parameters N_{nodes}, q^{add}, $q^{(0)}$, and T as given in Fig. 1. Red line indicates an exponential fit. (b), (c) Signal S_N of final stimulus as a function of age t_{N-1}^{age} before stimulus was applied. (b) and (c) show the data of Fig. 1(b) and Fig. 1(c), respectively. Blue lines indicate exponential fits.

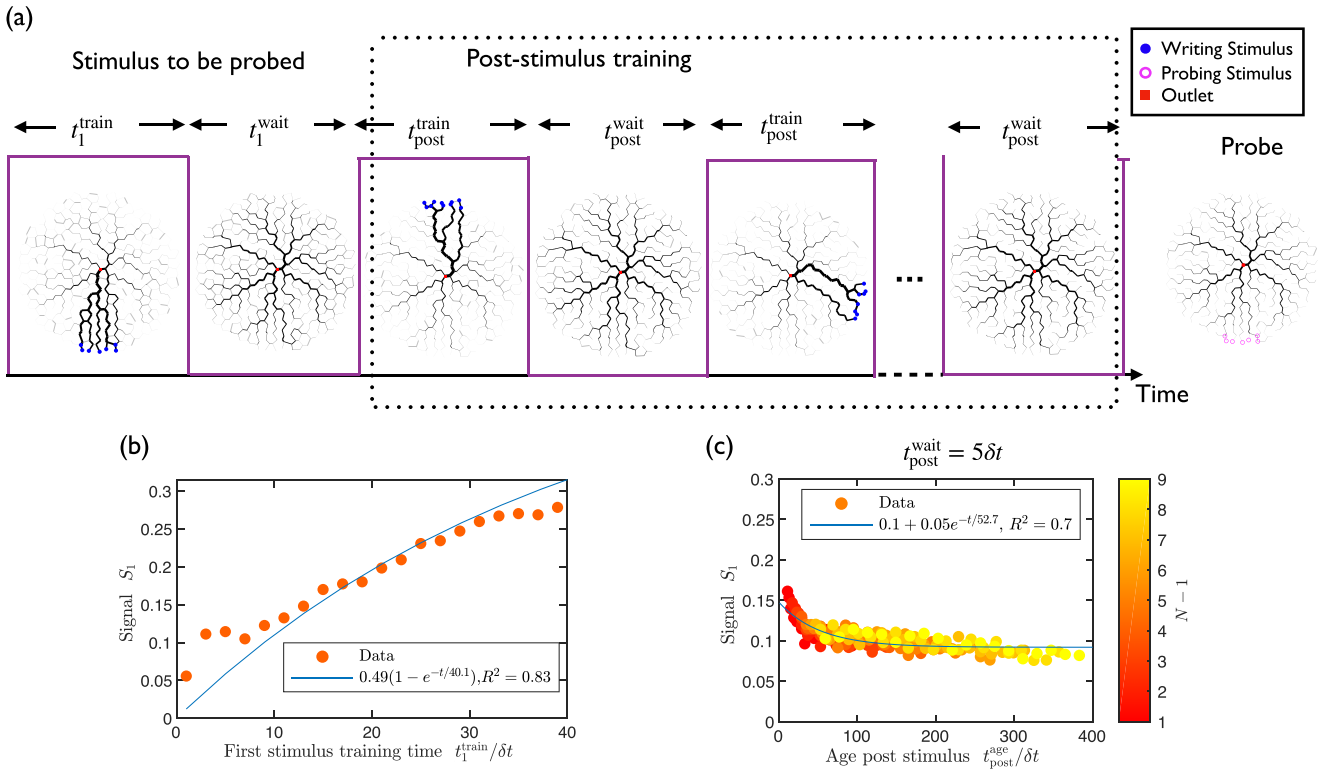

FIG. 3. Signal S_1 of first stimulus increases with training time and decreases with network age. (a) Snapshots of network, which is subjected to the first stimulus for t_1^{train}, relaxed for t_1^{wait}, and then $N-1$ stimuli are applied with $t_n^{\text{train}} = t_{\text{post}}^{\text{train}}$ and $t_n^{\text{wait}} = t_{\text{post}}^{\text{wait}}$ ($n > 1$, dotted box), until the first stimulus is probed. (b) S_1 as a function of t_1^{train} for $N = 5$ and $t_{\text{post}}^{\text{train}} = 5\delta t$. (c) S_1 as a function of $t_{\text{post}}^{\text{age}} = t_N^{\text{age}} - t_1^{\text{train}}$ for various N at $t_1^{\text{train}} = 10\delta t$. (b),(c) Blue lines indicate exponential fits. Parameters are $t_1^{\text{wait}} = t_{\text{post}}^{\text{wait}} = 5\delta t$ and are as given in Fig. 1.

described by an exponential decay,

$$S_N\left(t_{N-1}^{\text{age}}\right) \approx S_N^{\infty} + A_N \exp\left(-\frac{t_{N-1}^{\text{age}}}{\tau_{\text{pre}}}\right), \tag{6}$$

where $\tau_{\text{pre}} \approx 52\,\delta t$ denotes the timescale, with which prestimulation reduces the memory capacity of the final stimulus. The maximal memory capacity, $S_N^{\infty} + A_N \approx 0.22$ for $t_{N-1}^{\text{age}} = 0$, is significantly larger than the residual capacity, $S_N^{\infty} \approx 0.03$, consistent with the fact that prestimulation of the networks reduces the memory capacity. The fact that the exponential decay adequately describes the decreasing capacity suggests that only the total duration of prestimulation is important, while the details of the protocol are irrelevant; see the Supplemental Material [52], Sec. V. Consequently, younger networks allow for a larger memory signal of the final stimulus.

C. Training time dominates signal of first stimulus

To retain multiple memories, adaptive networks need to store information about all stimuli. We thus next investigate how information about earlier stimuli is retained and particularly focus on the first stimulus. To investigate the first stimulus in detail, we change the protocol to control the training parameters of the first stimulus separately from all the other stimuli; see Fig. 3(a). For simplicity, we use identical parameters for the other stimuli, $t_n^{\text{train}} = t_{\text{post}}^{\text{train}}$ and $t_n^{\text{wait}} = t_{\text{post}}^{\text{wait}}$ for $n = 2, \ldots, N$. The network is probed at the same location as the first stimulus to obtain the memory signal S_1 of the first stimulus. Figure 3(b) shows that S_1 increases with the training time of the first stimulus, t_1^{train}, and approaches zero for $t_1^{\text{train}} = 0$. S_1 again shows an exponential saturation,

$$S_1\left(t_1^{\text{train}}\right) \approx B_1\left[1 - \exp\left(-\frac{t_1^{\text{train}}}{\tau_{\text{train}}}\right)\right], \tag{7}$$

where τ_{train} is the training timescale and B_1 denotes the maximal signal for $t_1^{\text{train}} \to \infty$. Similar to our previous work [19], longer training leads to a stronger signal.

We next investigate how the signal of the first stimulus depends on subsequently applied stimuli. Figure 3(c) indicates that S_1 decays as the networks evolve further, similar to our previous study [19]. We find that S_1 only depends on the duration of evolution after the first training period, $t_{\text{post}}^{\text{age}} = t_N^{\text{age}} - t_1^{\text{train}}$, and not the precise details of the protocol. Moreover, S_1 again decays exponentially,

$$S_1\left(t_{\text{post}}^{\text{age}}\right) \approx S_1^{\infty} + A_1 \exp\left(-\frac{t_{\text{post}}^{\text{age}}}{\tau_{\text{post}}}\right), \tag{8}$$

where the coefficients have the same interpretation as in Eq. (6). Our fits indicate that $\tau_{\text{post}} \approx \tau_{\text{pre}}$, consistent with an intrinsic timescale of memory formation. Note that the residual memory capacity $S_1^{\infty} \approx 0.1$ is large, implying that subsequent training does not affect the signal very strongly. This is consistent with the picture that memory is stored by vanishing links that cannot be revived; see analytical and numerical

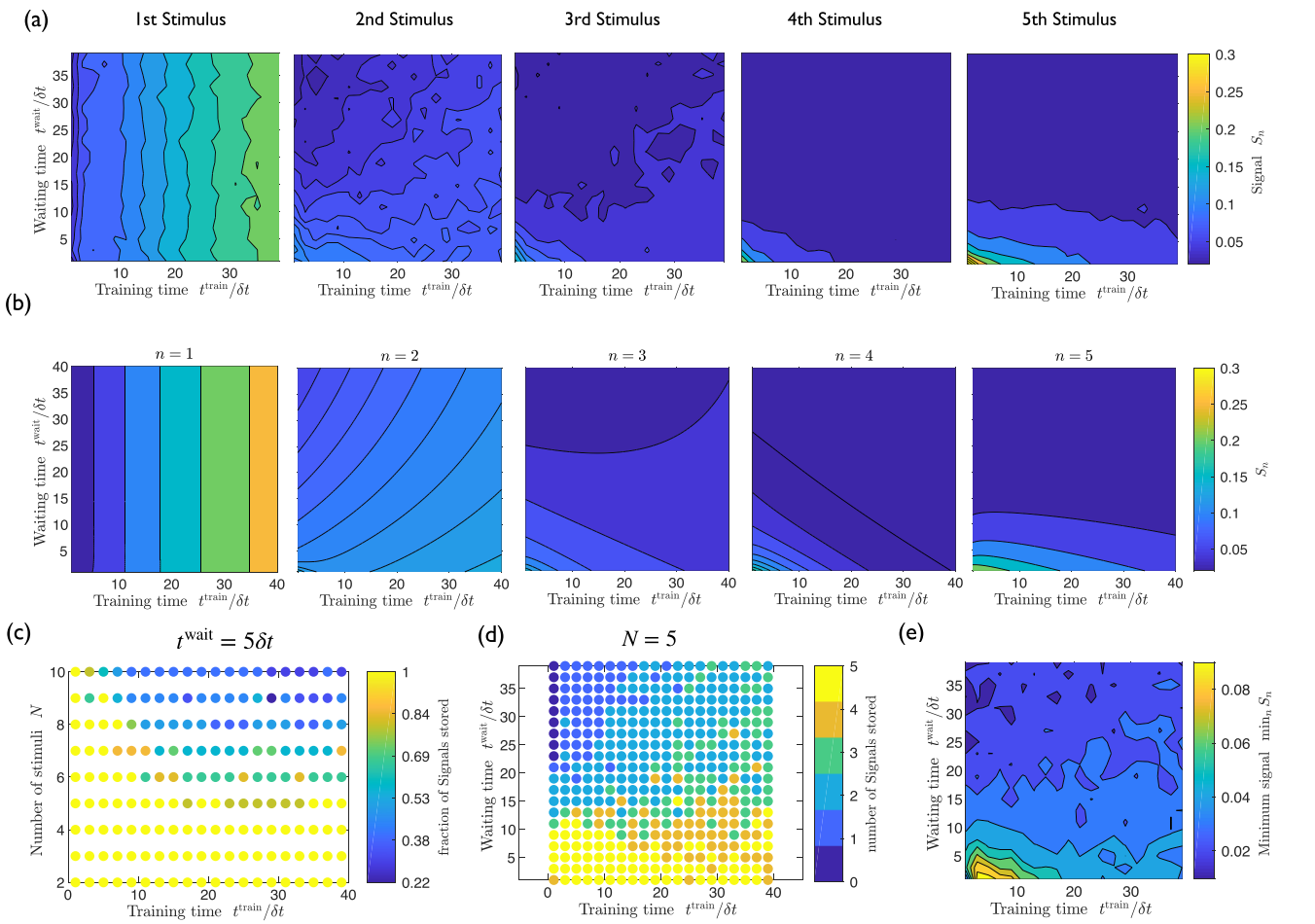

FIG. 4. Memory capacity depends on stimulation protocol parameters. (a) Numerically obtained signals S_n for all $N = 5$ stimuli as functions of training times t^{train} and waiting times t^{wait}. (b) Analytical prediction of S_n given by Eq. (9) for all stimuli as functions of t^{train} and t^{wait} for $N = 5$. (c) Fraction of stimuli with strong signal ($S_n > 0.04$) as a function of t^{train} and N for $t^{\text{wait}} = 5\delta t$. (d) Number of stimuli with $S_n > 0.04$ as a function of t^{train} and t^{wait} for $N = 5$. (e) Minimal signal $\min_n S_n$ of $N = 5$ stimuli as a function of t^{train} and t^{wait}. (a)–(e) Model parameters are as given in Fig. 1.

observations of the transitions phase between stimuli in the Supplemental Material [52], Secs. VI and VII. Taken together, we find that adaptive flow networks can store multiple memories.

D. Trade-off between age and training time limits memory capacity

We found that stimuli are imprinted most strongly when they are trained for a long time on a young network. These goals of long training times and young networks are contradictory for late stimuli which require young age for a strong signal, suggesting there must be a trade-off for best performance of imprinting multiple stimuli. We, thus, next investigate the memory capacity of networks, defined as the maximal number of different stimuli that can be imprinted and retrieved. To quantify memory capacity, we consider N nonoverlapping stimuli with identical stimulation parameters, $t_n^{\text{train}} = t^{\text{train}}$ and $t_n^{\text{wait}} = t^{\text{wait}}$ for $n = 1, ..., N$. We now also probe all stimuli locations to obtain a signal S_n for each stimulus. Figure 4(a) shows data for five stimuli as a function of t^{train} and t^{wait}. We recover that the signal S_1 of the first stimulus mainly depends on the training time t^{train} and is barely affected by the subsequent dynamics. Conversely, the signal of all other stimuli decreases with network age, i.e., with increasing t^{train} and t^{wait}. In particular, mid-timed stimuli have the weakest signals, suggesting that they are affected by both prestimuli aging as well as subsequent degradation.

We next develop an analytical prediction of the signal of all stimuli, motivated by the successful description of the signals of the first and last stimulus demonstrated above. We hypothesize that the signal of the nth stimulus is a combination of the prestimulus aging, described by Eq. (6), the actual training, described by Eq. (7), and poststimulus degradation effect described by Eq. (8). We show in Sec. VIII of the Supplemental Material [52] that a weighted sum of the prestimulus aging and training along with the poststimulus degradation effect adequately describes the data, which results in the prediction

$$S_n \approx \begin{cases} w^{\text{train}}\left(1 - e^{-\frac{t^{\text{train}}}{\tau_{\text{train}}}}\right) + W^{\text{post}} e^{-t^{\text{age}}_{\text{post}}/\tau_{\text{post}}}, & n = 1 \\ w^{\text{pre}} e^{-\frac{t^{\text{age}}_{n-1}}{\tau_{\text{pre}}}} + W^{\text{train}}\left(1 - e^{-\frac{t^{\text{train}}}{\tau_{\text{train}}}}\right) & \\ + W^{\text{post}} e^{-t^{\text{age}}_{\text{post}}/\tau_{\text{post}}}, & n > 1, \end{cases} \tag{9}$$

where t_n^{age} is given by Eq. (5) and

$$W^{\text{train}} = w_0^{\text{train}}(0.4n)^{1.5(1-n)}, \tag{10a}$$

$$W^{\text{post}} = 0.2e^{-t^{\text{train}}/\tau_{\text{coef}}}, \tag{10b}$$

$$\tau_{\text{post}} = 2.5 + 1.5(t^{\text{train}})^{0.5}; \tag{10c}$$

see the Supplemental Material [52], Sec. VIII. We choose the constants w^{pre}, w_0^{train}, and w^{train} to be 0.11, 0.11, and 0.5, respectively, to have values comparable to the fit parameters in Figs. 2 and 3.

This equation correctly captures that S_n decreases with the $n-1$ previously applied stimuli. Figure 4(b) shows that Eq. (9) also captures the qualitative features of the dependence on t^{train} and t^{wait}. However, this analytical description does not reproduce the quantitative features of the signal observed numerically because the signal is not just a linear superposition of the training and age impact; see the Supplemental Material [52], Sec. VIII. Even though more research is needed to obtain the exact dependency of the signal on training and age, we choose to use the simple function to draw mechanistic insights about the system. For instance, we observe that the ratio of the coefficient of training and the coefficient of age reduces with n, indicating that with every new stimulus application, the impact of age on memory formation becomes stronger. The advantage of the prediction is its simplicity. Moreover, the prediction is an *ad hoc* description of the parameter dependence and other choices are possible; see the Supplemental Material [52], Sec. VIII. The stimulation protocol is characterized by the three parameters n, t^{train}, and t^{wait}, while the almost identical τ_{coef}, τ_{pre}, and τ_{train} capture the characteristic timescale of network adaptation.

Finally, we investigate how many stimuli an adaptive network can store. We demand that a stored stimulus can be read out at a later time, implying that its signal exceeds a given threshold S_{thresh}, which captures uncertainties in the read-out apparatus as well as intrinsic noise. Figure 4(c) shows the fraction of stimuli that can be retrieved (where $S_n > S_{\text{thresh}}$) as a function of the total number of stimuli, N, and the training time t^{train}. In this case, large training times are detrimental since they age the network too much for later stimuli to be retrieved. Figure 4(d) shows the number of stimuli that can be retrieved as a function of the training and waiting time. The largest number of stimuli is stored for vanishing waiting times since this minimizes the aging of the network. To find optimal parameters for storing memory independent of the detection threshold S_{thresh} of the read-out apparatus, we show the minimal signal of all five stimuli for varying training and waiting time in Fig. 4(e). We observe a finite optimal training time, while a vanishing waiting time is best. Taken together, our analysis reveals the strong trade-off between writing stimuli for a sufficient duration and the resulting inevitable aging of the network that suppresses signals of subsequent stimuli.

IV. DISCUSSION

We showed that adaptive flow networks can store memory of multiple stimuli in the morphology of weak links, which cannot be revived in our model. Consequently, signatures of earlier stimuli are not destroyed by subsequent evolution, in contrast to the behavior of typical mechanical networks [38]. Such irreversible decay of links has also been observed in biological flow networks such as blood vasculature [53] and *P. polycephalum* [3] networks. Since older networks contain fewer strong links, which could shrink to store memory, the readout signal of each stimulus strongly decreases with the age of the network before the stimulus was written, which is similar to the memory plasticity observed in a disordered system [54,55]. Conversely, the signal strength increases with its training time, i.e., the duration the stimulus is presented, similar to memory formation by directed aging in mechanical networks [22,24]. Taken together, we showed that adaptive flow networks reach maximal capacity at an intermediate training time, which compromises between sufficiently imprinting and minimally aging.

Our work focuses on the simple situation that nonoverlapping stimuli are subsequently applied at the edge of flow networks of similar morphology. To describe realistic living flow networks, such as *Physarum* or our vasculature, our work will need to be extended in multiple directions: First, the overall network geometry will have an impact on how stimuli are stored. Work in mechanical networks [27,38] suggests that the internal timescales of flow networks and their memory capacity will depend on network size. Second, realistic systems deal with time-varying and potentially overlapping stimuli of various strengths. Third, living systems can grow and expand [56], implying that links can possibly regrow from their minimal size and new links can be added to the network. Taken together, it is likely that realistic adaptive flow networks show a dynamic behavior, storing information about stimuli on various timescales.

ACKNOWLEDGMENTS

This work was supported by the Max Planck Society. This project has received funding from the European Research Council (ERC) under the European Union's Horizon 2020 research and innovation program (Grant Agreement No. 947630, FlowMem).

[1] C. D. Murray, The physiological principle of minimum work: II. Oxygen exchange in capillaries, Proc. Natl. Acad. Sci. USA **12**, 299 (1926).

[2] L. Boddy, J. Wood, E. Redman, J. Hynes, and M. D. Fricker, Fungal network responses to grazing, Fungal Genet. Biol. **47**, 522 (2010).

[3] S. Marbach, K. Alim, N. Andrew, A. Pringle, and M. P. Brenner, Pruning to Increase Taylor Dispersion in *Physarum polycephalum* Networks, Phys. Rev. Lett. **117**, 178103 (2016).

[4] K. Alim, G. Amselem, F. Peaudecerf, M. P. Brenner, and A. Pringle, Random network peristalsis in *Physarum polycephalum* organizes fluid flows across an individual, Proc. Natl. Acad. Sci. USA **110**, 13306 (2013).

[5] W. W. Sugden, R. Meissner, T. Aegerter-Wilmsen, R. Tsaryk, E. V. Leonard, J. Bussmann, M. J. Hamm, W. Herzog, Y. Jin, L. Jakobsson, C. Denz, and A. F. Siekmann, Endoglin controls blood vessel diameter through endothelial cell shape changes in response to haemodynamic cues, Nat. Cell Biol. **19**, 653 (2017).

[6] Q. Chen, L. Jiang, C. Li, D. Hu, J.-W. Bu, D. Cai, and J.-L. Du, Haemodynamics-driven developmental pruning of brain vasculature in zebrafish, PLoS Biol. **10**, e1001374 (2012).

[7] D. Hu, D. Cai, and A. V. Rangan, Blood vessel adaptation with fluctuations in capillary flow distribution, PLoS ONE **7**, e45444 (2012).

[8] A. Tero, K. Yumiki, R. Kobayashi, T. Saigusa, and T. Nakagaki, Flow-network adaptation in Physarum amoebae, Theory Biosci. **127**, 89 (2008).

[9] A. Tero, S. Takagi, T. Saigusa, K. Ito, D. P. Bebber, M. D. Fricker, K. Yumiki, R. Kobayashi, and T. Nakagaki, Rules for biologically inspired adaptive network design, Science **327**, 439 (2010).

[10] S. Marbach, N. Ziethen, L. Bastin, F. K. Baüerle, and K. Alim, Vein fate determined by flow-based but time-delayed integration of network architecture, eLife **12**, e78100 (2023).

[11] N. Kamiya, R. D. Allen, and Y. Yoshimoto, Dynamic organization of Physarum plasmodium, Cell Motil. Cytoskeleton **10**, 107 (1988).

[12] S. Kuroda, S. Takagi, T. Nakagaki, and T. Ueda, Allometry in Physarum plasmodium during free locomotion: Size versus shape, speed and rhythm, J. Expt. Biol. **218**, 3729 (2015).

[13] M. Kramar and K. Alim, Encoding memory in tube diameter hierarchy of living flow network, Proc. Natl. Acad. Sci. USA **118**, e2007815118 (2021).

[14] K. Alim, Fluid flows shaping organism morphology, Philos. Trans. R. Soc. B **373**, 20170112 (2018).

[15] C. Gao, C. Liu, D. Schenz, X. Li, Z. Zhang, M. Jusup, Z. Wang, M. Beekman, and T. Nakagaki, Does being multi-headed make you better at solving problems? A survey of physarum-based models and computations, Phys. Life Rev. **29**, 1 (2019).

[16] M. Beekman and T. Latty, Brainless but multi-headed: Decision making by the acellular slime mould Physarum polycephalum, J. Mol. Biol. **427**, 3734 (2015).

[17] A. Tero, R. Kobayashi, and T. Nakagaki, Physarum solver: A biologically inspired method of road-network navigation, Physica A **363**, 115 (2006).

[18] T. Nakagaki, H. Yamada, and Á. Tóth, Maze-solving by an amoeboid organism, Nature (London) **407**, 470 (2000).

[19] K. Bhattacharyya, D. Zwicker, and K. Alim, Memory Formation in Adaptive Networks, Phys. Rev. Lett. **129**, 028101 (2022).

[20] M. Stern and A. Murugan, Learning without neurons in physical systems, Ann. Rev. Condens. Matter Phys. **14**, 417 (2023).

[21] D. R. Reid, N. Pashine, J. M. Wozniak, H. M. Jaeger, A. J. Liu, S. R. Nagel, and J. J. de Pablo, Auxetic metamaterials from disordered networks, Proc. Natl. Acad. Sci. USA **115**, E1384 (2018).

[22] N. Pashine, D. Hexner, A. J. Liu, and S. R. Nagel, Directed aging, memory, and nature's greed, Sci. Adv. **5**, eaax4215 (2019).

[23] J. W. Rocks, N. Pashine, I. Bischofberger, C. P. Goodrich, A. J. Liu, and S. R. Nagel, Designing allostery-inspired response in mechanical networks, Proc. Natl. Acad. Sci. USA **114**, 2520 (2017).

[24] D. Hexner, A. J. Liu, and S. R. Nagel, Periodic training of creeping solids, Proc. Natl. Acad. Sci. USA **117**, 31690 (2020).

[25] L. Yan, R. Ravasio, C. Brito, and M. Wyart, Architecture and coevolution of allosteric materials, Proc. Natl. Acad. Sci. USA **114**, 2526 (2017).

[26] S. Dillavou, M. Stern, A. J. Liu, and D. J. Durian, Demonstration of Decentralized, Physics-Driven Learning, Phys. Rev. Appl. **18**, 014040 (2022).

[27] J. W. Rocks, H. Ronellenfitsch, A. J. Liu, S. R. Nagel, and E. Katifori, Limits of multifunctionality in tunable networks, Proc. Natl. Acad. Sci. USA **116**, 2506 (2019).

[28] H. Yang and L. Ma, Multi-stable mechanical metamaterials with shape-reconfiguration and zero Poisson's ratio, Mater. Des. **152**, 181 (2018).

[29] G. Steinbach, D. Nissen, M. Albrecht, E. V. Novak, P. A. Sánchez, S. S. Kantorovich, S. Gemming, and A. Erbe, Bistable self-assembly in homogeneous colloidal systems for flexible modular architectures, Soft Matter **12**, 2737 (2016).

[30] K. Che, C. Yuan, J. Wu, H. Jerry Qi, and J. Meaud, Three-dimensional-printed multistable mechanical metamaterials with a deterministic deformation sequence, J. Appl. Mech. **84**, 011004 (2017).

[31] K. Bertoldi, V. Vitelli, J. Christensen, and M. Van Hecke, Flexible mechanical metamaterials, Nat. Rev. Mater. **2**, 17066 (2017).

[32] J. T. Overvelde, T. A. de Jong, Y. Shevchenko, S. A. Becerra, G. M. Whitesides, J. C. Weaver, C. Hoberman, and K. Bertoldi, A three-dimensional actuated origami-inspired transformable metamaterial with multiple degrees of freedom, Nat. Commun. **7**, 10929 (2016).

[33] J. L. Silverberg, J. H. Na, A. A. Evans, B. Liu, T. C. Hull, C. D. Santangelo, R. J. Lang, R. C. Hayward, and I. Cohen, Origami structures with a critical transition to bistability arising from hidden degrees of freedom, Nat. Mater. **14**, 389 (2015).

[34] S. Waitukaitis, R. Menaut, BryanGin-ge Chen, and M. van Hecke, Origami Multistability: From Single Vertices to Metasheets, Phys. Rev. Lett. **114**, 055503 (2015).

[35] Y. Yang, M. A. Dias, and D. P. Holmes, Multistable kirigami for tunable architected materials, Phys. Rev. Mater. **2**, 110601(R) (2018).

[36] H. Fu, K. Nan, W. Bai, W. Huang, K. Bai, L. Lu, C. Zhou, Y. Liu, F. Liu, J. Wang, M. Han, Z. Yan, H. Luan, Y. Zhang, Y. Zhang, J. Zhao, X. Cheng, M. Li, J. W. Lee, Y. Liu, D. Fang, X. Li, Y. Huang, Y. Zhang, and J. A. Rogers, Morphable 3D mesostructures and microelectronic devices by multistable buckling mechanics, Nat. Mater. **17**, 268 (2018).

[37] J. Z. Kim, Z. Lu, S. H. Strogatz, and D. S. Bassett, Conformational control of mechanical networks, Nat. Phys. **15**, 714 (2019).

[38] M. Stern, M. B. Pinson, and A. Murugan, Continual Learning of Multiple Memories in Mechanical Networks, Phys. Rev. X **10**, 031044 (2020).

[39] M. Stern, D. Hexner, J. W. Rocks, and A. J. Liu, Supervised Learning in Physical Networks: From Machine Learning to Learning Machines, Phys. Rev. X **11**, 021045 (2021).

[40] V. R. Anisetti, B. Scellier, and J. M. Schwarz, Learning by non-interfering feedback chemical signaling in physical networks, arXiv:2203.12098.

[41] K. Ito, D. Sumpter, and T. Nakagaki, Risk management in spatiotemporally varying field by true slime mold, Nonlinear Theor. Applic. IEICE **1**, 26 (2010).

[42] B. Meyer, C. Ansorge, and T. Nakagaki, The role of noise in self-organized decision making by the true slime mold Physarum polycephalum, PLoS ONE **12**, e0172933 (2017).

[43] W. J. Hacking, E. VanBavel, and J. A. Spaan, Shear stress is not sufficient to control growth of vascular networks: A model study, Am. J. Physiol. Heart Circ. Physiol. **270**, H364 (1996).

[44] S. Bohn and M. O. Magnasco, Structure, Scaling, and Phase Transition in the Optimal Transport Network, Phys. Rev. Lett. **98**, 088702 (2007).

[45] F. Corson, Fluctuations and Redundancy in Optimal Transport Networks, Phys. Rev. Lett. **104**, 048703 (2010).

[46] E. Katifori, G. J. Szöllosi, and M. O. Magnasco, Damage and Fluctuations Induce Loops in Optimal Transport Networks, Phys. Rev. Lett. **104**, 048704 (2010).

[47] D. Hu and D. Cai, Adaptation and Optimization of Biological Transport Networks, Phys. Rev. Lett. **111**, 138701 (2013).

[48] D. Peak, J. D. West, S. M. Messinger, and K. A. Mott, Evidence for complex, collective dynamics and emergent, distributed computation in plants, Proc. Natl. Acad. Sci. USA **101**, 918 (2004).

[49] B. Klitzman, D. N. Damon, R. J. Gorczynski, and B. R. Duling, Augmented tissue oxygen supply during striated muscle contraction in the hamster. Relative contributions of capillary recruitment, functional dilation, and reduced tissue PO2, Circ. Res. **51**, 711 (1982).

[50] J. B. Delashaw and B. R. Duling, A study of the functional elements regulating capillary perfusion in striated muscle, Microvasc. Res. **36**, 162 (1988).

[51] T. E. Sweeney and I. H. Sarelius, Arteriolar control of capillary cell flow in striated muscle, Circ. Res. **64**, 112 (1989).

[52] See Supplemental Material at http://link.aps.org/supplemental/10.1103/PhysRevE.107.034407 for additional data, details of governing dynamics of network links and details of the analytical approximation of memory readout signal.

[53] A. R. Pries and T. W. Secomb, Making microvascular networks work: Angiogenesis, remodeling, and pruning, Physiology **29**, 446 (2014).

[54] N. C. Keim and S. R. Nagel, Generic Transient Memory Formation in Disordered Systems with Noise, Phys. Rev. Lett. **107**, 010603 (2011).

[55] J. D. Paulsen, N. C. Keim, and S. R. Nagel, Multiple Transient Memories in Experiments on Sheared Non-Brownian Suspensions, Phys. Rev. Lett. **113**, 068301 (2014).

[56] H. Ronellenfitsch and E. Katifori, Global Optimization, Local Adaptation, and the Role of Growth in Distribution Networks, Phys. Rev. Lett. **117**, 138301 (2016).